Computer Assisted Mechanics and Engineering Sciences, 7: 767–780, 2000.


# Embedded discontinuities for 3D mode-I and mode-II failure modelling

Garth N. Wells and Lambertus J. Sluys
*Koiter Institute Delft, Delft University of Technology*
*P.O. Box 5048, 2600 GA Delft, The Netherlands*

(Received November 10, 1999)

The incorporation of displacement discontinuities in finite elements is examined. The incorporation of displacement discontinuities allows the use of discrete constitutive models in a continuum framework in order to avoid the mesh sensitivity of classical continuum models when strain softening is introduced. The procedure for building discontinuities into finite elements is examined, as well as two classes of constitutive models for mode-I and mode-II failure analysis. The performance of the model is illustrated with three-dimensional examples.

## 1. Introduction

As computational tools have developed, increased emphasis has been placed on the proper modelling of the complete response of materials from the elastic stage through to full loss of integrity. Attempts to model the full loading cycle of structures has exposed deficiencies in classical models. In overcoming the deficiencies of classical models, the approaches adopted for the modelling of localised material failure can be placed in two distinct groups: discrete and continuum. Each of the two groups possess strengths and weaknesses. In many materials, near the peak load narrow zones of intense straining or of damaged material appear. At some point after further loading, obvious, discrete discontinuities develop before complete failure. These physical observations of discrete discontinuities are of course the motivation behind discrete approaches such as linear elastic fracture mechanics. However, before the appearance of discrete cracks, significant inelastic deformation usually occurs in a material.

The application of discrete failure models poses significant computational difficulties. Within the finite element method, discontinuities at inter-element boundaries [10] lead to obvious dependency on the mesh structure. Attempts to overcome this rely on intensive re-meshing strategies to align the finite element mesh with the crack path [14]. Alternative techniques, especially the element-free Galerkin method, have been used to include discrete displacement jumps that are not required to follow predefined paths [3], but generally lack the efficiency of the finite element method. The strength of discrete models is the ability to model the genuine separation that occurs in the late stages of loading. Also, particularly for crack propagation problems, discrete models are able to produce naturally the anisotropic nature of a cracked medium.

The alternative approach, applying continuum concepts of stress and strain, also faces significant difficulties. Application of classical continuum models with strain softening leads to results that are highly mesh dependent in terms of both element size and mesh structure. In the presence of strain softening the underlying governing differential equations become ill-posed. The practical consequence is that the predicted failure zone is of zero width, leading upon mesh refinement to the spurious case of complete failure with zero energy dissipation. The collapsing failure zone as predicted by classical models calls for the inclusion of an extra parameter in the material description; a so-called internal length scale (incidentally the need for an internal length scale has been

long recognised in fracture mechanics). An internal length scale, which describes the size of the failure zone, can be included by considering non-local terms [9], higher order strain gradients [2] or time derivatives (viscosity) [13] in the continuum description. The governing differential equations for these models remain well-posed, leading to results that are objective with respect to spatial discretisation. These models however require that the typical finite element size in the failure zone is significantly smaller than the internal length scale. For many realistic problems, this limits the practicality of such models. Also, while such models can reproduce the material response near the peak load, it can be difficult to introduce anisotropy as a result of softening and to model the late stages of failure where genuine material separation occurs in the real problem.

The approach developed here is a hybrid between discrete and continuum methods. Effectively, a discrete displacement jump is added to the underlying continuum description [1, 4, 5, 8, 12, 16]. Numerically, the displacement jump is added by introducing discontinuous functions to finite elements. Then, while discrete constitutive relationships are applied across the displacement jump, the orientation of the discontinuity planes is determined by the local stress or strain field, rather than by any predefined directions. This approach is ideal for large scale calculations, particularly in three-dimensions, where the typical finite element size is significantly larger than any internal length scale of the material.

In order to include *strong* (displacement) discontinuities, a method for enhancing three-dimensional solid continuum finite elements is shown by extending the variational statements to include a displacement jump. The exact form of the element enhancements is determined by imposing traction continuity and considering the kinematic requirements to overcome mesh alignment dependency. Following the element formulation, two classes of discrete models are examined, one particularly suitable for mode-I type failure and the second for mode-II type failure. The two different constitutive models are then applied to three-dimensional problems.

## 2. Kinematics of a strong discontinuity

To develop a kinematic description of a body crossed by a material discontinuity, consider a body $\Omega$ crossed by a single discontinuity (Fig. 1). The discontinuity in denoted $\Gamma_d$. It is useful at this point to define a sub-domain $\Omega_d$ ($\Omega_d \in \Omega$). The sub-domain $\Omega_d$ is centred on the discontinuity. The normal vector to the discontinuity is denoted $\mathbf{n}$.

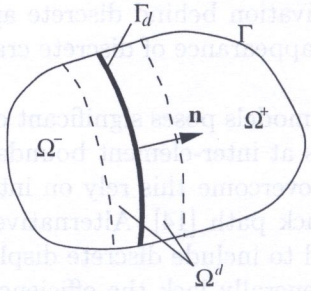


**Fig. 1.** Body crossed by a material discontinuity

### 2.1. Decomposition of the displacement field

The displacement field $\mathbf{u}(\mathbf{x}, t)$ for the body shown in Fig. 1 can be decomposed into two parts: one containing regular, continuous parts ($\hat{\mathbf{u}}$) and the other providing a displacement jump across $\Gamma_d$ ($\mathcal{H}_{\Gamma_d} [\![\mathbf{u}]\!]$),

$$\mathbf{u}(\mathbf{x}, t) = \hat{\mathbf{u}}(\mathbf{x}, t) + \mathcal{H}_{\Gamma_d} [\![\mathbf{u}(\mathbf{x}, t)]\!] \,. \tag{1}$$

The displacement jump is provided via the Heaviside function centred on the discontinuity ($\mathcal{H}_{\Gamma_d} = 1$ if $\mathbf{x} \in \Omega^+$, $\mathcal{H}_{\Gamma_d} = 0$ if $\mathbf{x} \in \Omega^-$) operating on a function $[\![\mathbf{u}(\mathbf{x},t)]\!]$ that is continuous over the body. The components of the displacement jump at the discontinuity are given by $[\![\mathbf{u}(\mathbf{x},t)]\!]_{\mathbf{x}\in\Gamma_d}$.

For later finite element implementation, it is advantageous to refine the displacement decomposition given in (1). Without any loss of generality, it is possible to construct the decomposition such that *only* the regular part of the displacement field is non-zero on the boundary of $\Omega$ [6]. Then, boundary conditions need only be applied on the regular part of the displacement field,

$$\mathbf{u}(\mathbf{x},t) = \hat{\mathbf{u}}(\mathbf{x},t) + (\mathcal{H}_{\Gamma_d} - \varphi(\mathbf{x}))\,[\![\mathbf{u}(\mathbf{x},t)]\!]\,. \tag{2}$$

The function $\varphi(\mathbf{x})$ in (2) is a continuous function that obeys:

$$\varphi(\mathbf{x}) = \begin{cases} 1 & \mathbf{x} \in \Omega^+ \backslash \Omega^d\,, \\ 0 & \mathbf{x} \in \Omega^- \backslash \Omega^d\,. \end{cases} \tag{3}$$

The displacement decomposition for the one-dimensional case is shown in Fig. 2.

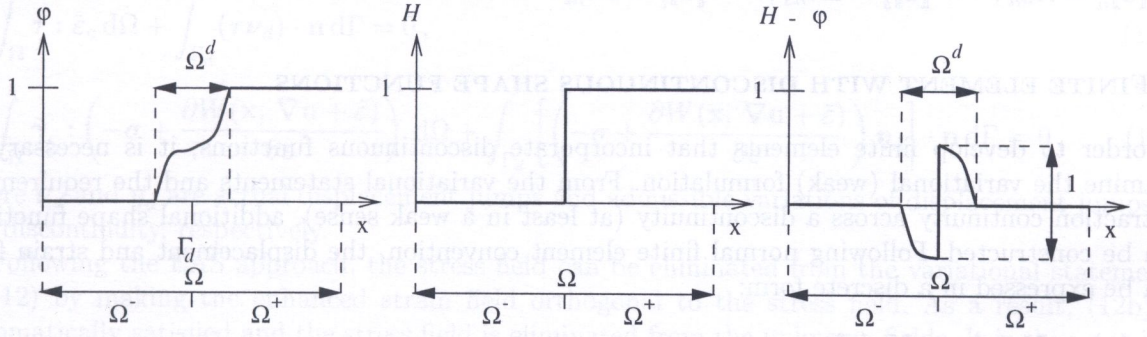


**Fig. 2.** 1-D displacement decomposition

The strain field for a body crossed by a discontinuity is found by taking the gradient of (2). Infinitely small strains are assumed throughout so all gradients ($\nabla$) are taken to be the symmetric part only (for an extension to finite strains, see Armero and Garikipati, [1]). Taking the gradient of (2),

$$\varepsilon(\mathbf{x},t) = \nabla\mathbf{u}(\mathbf{x},t) = \underbrace{\nabla\hat{\mathbf{u}} + \mathcal{H}_{\Gamma_d}(\nabla\,[\![\mathbf{u}(\mathbf{x},t)]\!]) - ([\![\mathbf{u}(\mathbf{x},t)]\!] \otimes \nabla\varphi(\mathbf{x}))^s - \varphi(\mathbf{x})(\nabla\,[\![\mathbf{u}(\mathbf{x},t)]\!])}_{\text{bounded}}$$
$$+ \underbrace{\delta_{\Gamma_d}([\![\mathbf{u}(\mathbf{x},t)]\!] \otimes \mathbf{n}(\mathbf{x}))^s}_{\text{unbounded}}, \tag{4}$$

where $\delta_{\Gamma_d}$ is the Dirac-delta distribution centred on the discontinuity. Grouping all the regular (bounded) parts of the strain field together, (4) can be expressed:

$$\varepsilon(\mathbf{x},t) = \bar{\varepsilon} + \delta_{\Gamma_d}([\![\mathbf{u}(\mathbf{x},t)]\!] \otimes \mathbf{n}(\mathbf{x}))^s. \tag{5}$$

## 2.2. Basis at the discontinuity

It can be shown that for an orthogonal basis at the discontinuity, with $\mathbf{n}$ the normal to the discontinuity and $\mathbf{s}$ and $\mathbf{t}$ two mutually orthogonal (unit) vectors in the plane of the discontinuity,

that [7]:

$$\begin{aligned}
\mathbf{s}\cdot(\llbracket\mathbf{u}\rrbracket\otimes\mathbf{n})\,\mathbf{s} &= 0,\\
\mathbf{t}\cdot(\llbracket\mathbf{u}\rrbracket\otimes\mathbf{n})\,\mathbf{t} &= 0,\\
\mathbf{s}\cdot(\llbracket\mathbf{u}\rrbracket\otimes\mathbf{n})\,\mathbf{t} &= 0,\\
\mathbf{n}\cdot(\llbracket\mathbf{u}\rrbracket\otimes\mathbf{n})\,\mathbf{n} &= \llbracket\mathbf{u}\rrbracket\cdot\mathbf{n},\\
\mathbf{n}\cdot(\llbracket\mathbf{u}\rrbracket\otimes\mathbf{n})\,\mathbf{s} &= \tfrac{1}{2}\llbracket\mathbf{u}\rrbracket\cdot\mathbf{s},\\
\mathbf{n}\cdot(\llbracket\mathbf{u}\rrbracket\otimes\mathbf{n})\,\mathbf{t} &= \tfrac{1}{2}\llbracket\mathbf{u}\rrbracket\cdot\mathbf{t},
\end{aligned} \tag{6}$$

Using the results in (6), the basis components at a discontinuity can be written:

$$(\llbracket\mathbf{u}\rrbracket\otimes\mathbf{n})^s = \begin{bmatrix} A_{nn} & A_{nt} & A_{ns} \\ A_{nt} & 0 & 0 \\ A_{ns} & 0 & 0 \end{bmatrix}. \tag{7}$$

The individual components of the displacement jump vector are written:

$$\llbracket u\rrbracket_n = A_{nn}\,, \qquad \llbracket u\rrbracket_s = 2A_{ns}\,, \qquad \llbracket u\rrbracket_t = 2A_{nt}\,. \tag{8}$$

## 3. Finite element with discontinuous shape functions

In order to develop finite elements that incorporate discontinuous functions, it is necessary to examine the variational (weak) formulation. From the variational statements and the requirement of traction continuity across a discontinuity (at least in a weak sense), additional shape functions can be constructed. Following normal finite element convention, the displacement and strain field can be expressed in a discrete form:

$$\mathbf{u}(\mathbf{x}) = \mathbf{N}_a(\mathbf{x})\,\mathbf{a} + \mathbf{N}_\alpha(\mathbf{x})\,\boldsymbol{\alpha}\,, \tag{9a}$$

$$\varepsilon(\mathbf{x}) = \underbrace{\mathbf{B}(\mathbf{x})\,\mathbf{a}}_{\text{regular}} + \underbrace{\mathbf{G}(\mathbf{x})\,\boldsymbol{\alpha}}_{\text{enhanced}}\,, \tag{9b}$$

where $\mathbf{a}$ are the regular nodal displacements, $\boldsymbol{\alpha}$ are the displacements (enhanced) associated with a discontinuity (displacement jump vector across a discontinuity), $\mathbf{N}_a$ and $\mathbf{B}$ are the normal displacement and strain interpolation matrices and $\mathbf{N}_\alpha$ and $\mathbf{G}$ are the displacement and strain interpolation matrices associated with the enhanced degrees of freedom.

The decomposition of the strain field allows the use of so-called *enhanced assumed strains* (EAS) [11] where the strain field is decomposed into compatible ($\boldsymbol{\nabla}\mathbf{u}$) and incompatible ($\tilde{\varepsilon}$) parts.

### 3.1. Mixed variational formulation

It is convenient to begin the embedded element formulation from a modified form of the Hu–Washizu three-field variational statements that allows for *enhanced* strains [11]

$$\int_\Omega \boldsymbol{\nabla}\boldsymbol{\eta} : \frac{\partial W(\mathbf{x},\,\boldsymbol{\nabla}\mathbf{u}+\tilde{\varepsilon})}{\partial\varepsilon}\,\mathrm{d}\Omega - W^{\text{ext}}(\boldsymbol{\eta}) = 0\,, \tag{10a}$$

$$\int_\Omega \boldsymbol{\tau} : \tilde{\varepsilon}\,\mathrm{d}\Omega = 0\,, \tag{10b}$$

$$\int_\Omega \tilde{\boldsymbol{\gamma}} : \left(-\boldsymbol{\sigma} + \frac{\partial W(\mathbf{x},\,\boldsymbol{\nabla}\mathbf{u}+\tilde{\varepsilon})}{\partial\varepsilon}\right)\mathrm{d}\Omega = 0\,, \tag{10c}$$

where $(\boldsymbol{\eta}, \tilde{\boldsymbol{\gamma}}, \boldsymbol{\tau}) \in (V \times \tilde{E} \times S)$ are variations of displacements, enhanced strains and stresses respectively with $(V \times \tilde{E} \times S)$ the spaces of admissible displacements, enhanced strains and stresses. The actual displacements, strains and displacements are denoted $(\mathbf{u}, \boldsymbol{\varepsilon}, \boldsymbol{\sigma}) \in (V \times E \times S)$ with the actual strain field being the sum of compatible and incompatible parts ($\boldsymbol{\varepsilon} = \nabla\mathbf{u} + \tilde{\boldsymbol{\varepsilon}}$) and the stresses coming from the constitutive law are given by $\partial W(\mathbf{x}, \nabla\mathbf{u} + \tilde{\boldsymbol{\varepsilon}})/\partial\boldsymbol{\varepsilon}$. The external work is given by $W^{\text{ext}}$.

From the displacement decomposition in Section 2.1 it was shown that as a result of a displacement jump, Dirac-delta distributions must arise the enhanced strain field. Considering this, the enhanced strains can also be decomposed into a bounded and an unbounded part.

$$\tilde{\boldsymbol{\varepsilon}} = \tilde{\boldsymbol{\varepsilon}}_c + \tilde{\boldsymbol{\varepsilon}}_d \,. \tag{11}$$

The subscript $c$ is the above equation denotes the continuous, bounded part and the subscript $d$ denotes the discontinuous, unbounded part. The discontinuous part is non-zero only on the discontinuity $\Gamma_d$. Using properties of the Dirac-delta distribution ($\int_\Omega \phi\, \delta_{\Gamma_d}\, \mathrm{d}\Omega = \int_{\Gamma_d} \phi\, \mathrm{d}\Gamma$), the variational statements in (10) can be extended for the case of a body crossed by a discontinuity [5, 16],

$$\int_\Omega \nabla\boldsymbol{\eta} : \frac{\partial W(\mathbf{x}, \nabla\mathbf{u} + \tilde{\boldsymbol{\varepsilon}})}{\partial\boldsymbol{\varepsilon}}\, d\Omega - W^{\text{ext}}(\boldsymbol{\eta}) = 0 \,, \tag{12a}$$

$$\int_\Omega \boldsymbol{\tau} : \tilde{\boldsymbol{\varepsilon}}_c\, \mathrm{d}\Omega + \int_{\Gamma_d} (\boldsymbol{\tau}\boldsymbol{\nu}_d) \cdot \mathbf{n}\, \mathrm{d}\Gamma = 0 \,, \tag{12b}$$

$$\int_\Omega \tilde{\boldsymbol{\gamma}}_c : \left(-\boldsymbol{\sigma} + \frac{\partial W(\mathbf{x}, \nabla\mathbf{u} + \tilde{\boldsymbol{\varepsilon}})}{\partial\boldsymbol{\varepsilon}}\right) \mathrm{d}\Omega + \int_{\Gamma_d} \left[\left(-\boldsymbol{\sigma} + \frac{\partial W(\mathbf{x}, \nabla\mathbf{u} + \tilde{\boldsymbol{\varepsilon}})}{\partial\boldsymbol{\varepsilon}}\right) \boldsymbol{\eta}_d\right] \cdot \mathbf{n}\, \mathrm{d}\Gamma = 0 \,, \tag{12c}$$

where $\boldsymbol{\nu}_d$ and $\boldsymbol{\eta}_d$ are actual displacement jumps and admissible variations of displacement jumps at the discontinuity, respectively.

Following the EAS approach, the stress field can be eliminated from the variational statements in (12) by making the enhanced strain field orthogonal to the stress field. As a result, (12b) is automatically satisfied and the stress field is eliminated from the unknown fields. It is then possible to rephrase (12c) as:

$$\int_{\Omega\setminus\Gamma_d} \tilde{\boldsymbol{\gamma}}_c : \frac{\partial W(\mathbf{x}, \nabla\mathbf{u} + \tilde{\boldsymbol{\varepsilon}})}{\partial\boldsymbol{\varepsilon}}\, \mathrm{d}\Omega + \int_{\Gamma_d} \left(\frac{\partial W(\mathbf{x}, \nabla\mathbf{u} + \tilde{\boldsymbol{\varepsilon}})}{\partial\boldsymbol{\varepsilon}}\, \boldsymbol{\eta}_d\right) \cdot \mathbf{n}\, \mathrm{d}\Gamma = 0 \tag{13}$$

Now the virtual work equation (12a) and (13) provide two weak governing equations:

$$\int_\Omega \nabla\boldsymbol{\eta} : \frac{\partial W(\mathbf{x}, \nabla\mathbf{u} + \tilde{\boldsymbol{\varepsilon}})}{\partial\boldsymbol{\varepsilon}}\, \mathrm{d}\Omega = W^{\text{ext}}(\boldsymbol{\eta}) \,, \tag{14a}$$

$$\int_{\Omega_e\setminus\Gamma_d} \tilde{\boldsymbol{\gamma}}_c : \frac{\partial W(\mathbf{x}, \nabla\mathbf{u} + \tilde{\boldsymbol{\varepsilon}})}{\partial\boldsymbol{\varepsilon}}\, \mathrm{d}\Omega + \int_{\Gamma_d} \mathbf{t}_{\Gamma_d,e} \cdot \boldsymbol{\eta}_d\, \mathrm{d}\Gamma = 0 \,, \tag{14b}$$

where $\mathbf{t}_{\Gamma_d,e}$ comes from a discrete traction–separation law and (14b) applies to all elements crossed by a discontinuity. The domain $\Omega_e$ indicates an element.

For a straight discontinuity within an element ($\mathbf{n}$ is constant over $\Omega_e$) with a constant strain field on $\Omega_e$ (this is true for constant strain elements) and considering that in order to satisfy the patch test [15] Eq. (13) must hold for a constant stress field, (13) can be integrated explicitly over an element $\Omega_e$

$$V_e\tilde{\boldsymbol{\gamma}}_c + A_e(\mathbf{n} \otimes \boldsymbol{\eta}_d)^s = \mathbf{0} \tag{15}$$

where $V_e$ is the volume of an element and $A_e$ is the area of the discontinuity plane through an element. Rearranging (15) gives the form of the continuous part of the enhanced strain field away from the discontinuity

$$\tilde{\boldsymbol{\gamma}}_c = -\frac{A_e}{V_e}(\mathbf{n} \otimes \boldsymbol{\eta}_d)^s \,. \tag{16}$$

### 3.2. Discretised form

The discrete form of the weak equilibrium equations in (14) can written:

$$\int_{\Omega} \mathbf{B}^{\mathrm{T}} \boldsymbol{\sigma} \, \mathrm{d}\Omega = \mathbf{f}^{\mathrm{ext}}, \tag{17a}$$

$$\int_{\Omega_e} \mathbf{G}^{*\mathrm{T}} \boldsymbol{\sigma} \, \mathrm{d}\Omega + \int_{\Gamma_{d,e}} \mathbf{t}_e \, \mathrm{d}\Gamma = \mathbf{0}, \tag{17b}$$

where $\mathbf{f}^{\mathrm{ext}}$ is the external force vectorand $\mathbf{G}^*$ is an interpolation matrix formed considering (16). From (16), the matrix $\mathbf{G}^*$ for an element must be of the form:

$$\mathbf{G}_e^* = -\frac{A_e}{V_e} \begin{bmatrix} n_x & 0 & 0 \\ 0 & n_y & 0 \\ 0 & 0 & n_z \\ n_y & n_x & 0 \\ 0 & n_z & n_y \\ n_z & 0 & n_x \end{bmatrix} \tag{18}$$

where $(n_x\,,\, n_y\,,\, n_z)$ are the components of the unit normal to the discontinuity passing through the element.

Artificial numerical parameters, as used in so-called 'crack bandwidth' approaches, have been avoided through the inclusion and later explicit integration of Dirac-delta distributions. By maintaining the Dirac-delta distributions through the derivation and eventual explicit integration, approximation of the unbounded distribution [5, 8] is avoided. Approximating the Dirac-delta distribution allows the direct application of continuum constitutive models but may lead to a loss of robustness and under some circumstances stress locking [16].

There is however nothing in the enhanced strain interpolation to overcome the mesh alignment dependency of classical continuum models. To assist in overcoming mesh-alignment dependency, it is necessary to enhance the finite element shape from a kinematic perspective. To do this, the displacement decomposition (2) is considered again. If the continuous part of the displacement field is represented by the regular finite element shape functions, an interpolation matrix $\mathbf{G}_e$ over an element can be formed by taking the gradient of the last term of (2).

$$\mathbf{G}_e(\mathbf{x}) = \begin{bmatrix} \delta_{\Gamma_d} n_x - \frac{\partial \varphi(\mathbf{x})}{\partial x} & 0 & 0 \\ 0 & \delta_{\Gamma_d} n_y - \frac{\partial \varphi(\mathbf{x})}{\partial y} & 0 \\ 0 & 0 & \delta_{\Gamma_d} n_z - \frac{\partial \varphi(\mathbf{x})}{\partial z} \\ \delta_{\Gamma_d} n_y - \frac{\partial \varphi(\mathbf{x})}{\partial y} & \delta_{\Gamma_d} n_x - \frac{\partial \varphi(\mathbf{x})}{\partial x} & 0 \\ 0 & \delta_{\Gamma_d} n_z - \frac{\partial \varphi(\mathbf{x})}{\partial z} & \delta_{\Gamma_d} n_y - \frac{\partial \varphi(\mathbf{x})}{\partial y} \\ \delta_{\Gamma_d} n_z - \frac{\partial \varphi(\mathbf{x})}{\partial z} & 0 & \delta_{\Gamma_d} n_x - \frac{\partial \varphi(\mathbf{x})}{\partial x} \end{bmatrix}. \tag{19}$$

For robust implementation, it is necessary to modify (19) such that $\varphi(\mathbf{x})$ is constant along the discontinuity within an element [17].

Now, in order to utilise the kinematic superiority of the interpolations $\mathbf{G}$ and enforce traction continuity in a weak sense using the EAS interpolations $\mathbf{G}^*$, a non-symmetric formulation is used where the kinematic interpolations are used for the stress update ($\dot{\boldsymbol{\sigma}} = \mathbf{D}(\mathbf{B}\dot{\mathbf{a}} + \mathbf{G}\dot{\boldsymbol{\alpha}})$) and the EAS interpolations are used as test functions (in general $\mathbf{G} \neq \mathbf{G}^*$). Effectively, the space of admissible strain variations is not necessarily the same as the space of admissible strains. This is unlike normal Galerkin procedures where the space of admissible functions and the space of admissible variations of the functions are the same which results in a symmetric tangent operator if the material tangent is symmetric.

### *3.2.1. Element tangent operator*

By linearising the rate form of the stress–strain relationship and substituting it into the discrete weak governing equations (17) it is possible to form the stiffness tangent for an element

$$\begin{bmatrix} \mathbf{K}_{bb,e} & \mathbf{K}_{bg,e} \\ \mathbf{K}_{g^*b,e} & \mathbf{K}_{g^*g,e} + \mathbf{K}_{t,e} \end{bmatrix} \begin{Bmatrix} \mathrm{d}\mathbf{a}_e \\ \mathrm{d}\boldsymbol{\alpha}_e \end{Bmatrix} = \begin{Bmatrix} \mathbf{f}^{\mathrm{ext}}_{u,e} \\ \mathbf{0} \end{Bmatrix} - \begin{Bmatrix} \mathbf{f}^{\mathrm{int}}_{u,e} \\ \mathbf{f}^{\mathrm{int}}_{\alpha,e} \end{Bmatrix} \tag{20}$$

where

$$\begin{aligned} \mathbf{K}_{bb,e} &= \int_{\Omega_e} \mathbf{B}_e^{\mathrm{T}} \mathbf{D} \mathbf{B}_e \, \mathrm{d}\Omega \,, \\ \mathbf{K}_{bg,e} &= \int_{\Omega_e} \mathbf{B}_e^{\mathrm{T}} \mathbf{D} \mathbf{G}_e \, \mathrm{d}\Omega \,, \\ \mathbf{K}_{g^*b,e} &= \int_{\Omega_e} \mathbf{G}_e^{*\mathrm{T}} \mathbf{D} \mathbf{B}_e \, \mathrm{d}\Omega \,, \\ \mathbf{K}_{g^*g,e} &= \int_{\Omega_e} \mathbf{G}_e^{*\mathrm{T}} \mathbf{D} \mathbf{G}_e \, \mathrm{d}\Omega \,, \\ \mathbf{K}_{t,e} &= \int_{\Gamma_e} \mathbf{T}_e \, \mathrm{d}\Gamma \,, \end{aligned} \tag{21}$$

and $\mathbf{T}_e$ is the matrix that relates displacements and tractions at the discontinuity ($\dot{\mathbf{t}}_e = \mathbf{T}_e \dot{\boldsymbol{\alpha}}_e$). Note that $\mathbf{G}_e$ contains only the regular parts of (19). The enhanced modes ($\boldsymbol{\alpha}_e$) can be solved for at element level through static condensation. It can be seen that irrespective of the material model used, the element stiffness matrix is non-symmetric as a result of the combined EAS–kinematic approach.

## 4. Discrete constitutive models

In this section, two distinct groups of discrete constitutive models are examined. The first, which is applicable to mode-I type failure, is based on phenomenological consideration of crack opening separation, crack sliding and the tractions transfered across a crack [17]. The discontinuity direction comes from principal stress (or strains) directions. The second constitutive model evolves from the analysis of bifurcation and strain localisation in an elastoplastic continuum. By including Dirac-delta distributions in the strain field, it is possible to show that classical continuum plasticity models are compatible with displacement discontinuities in the presence of strain softening. Here an associative von Mises model is developed in a discrete form for the analysis of mode-II failure. All of the models here are constructed in a local coordinate system relative to the discontinuity plane (see Fig. 3). Also in the models developed here, an elastic response is assumed away from the discontinuity.

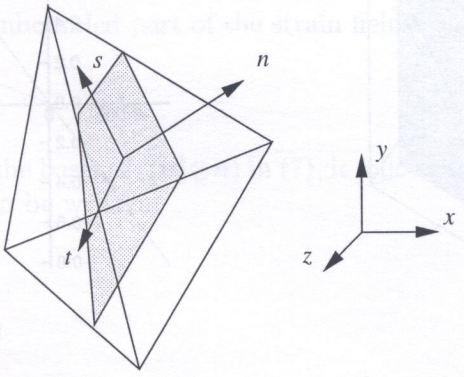


**Fig. 3.** Local $n$, $s$, $t$ coordinate system within a tetrahedral element

### 4.1. Cohesive crack type model

For the modelling of brittle fracture, a simple damage type model has been applied. If, at the end of a loading step, the maximum tensile principal stress has exceeded the tensile strength of the material ($f_t$), a discontinuity is introduced with the normal to the discontinuity in the direction of the maximum tensile principal stress. Discontinuities are introduced only at the end of a converged step to avoid the introduction of discontinuities into non-equilibrium states and to maintain the quadratic convergence behaviour of the full Newton-Raphson solution procedure.

Once a discontinuity has been introduced, the maximum crack opening displacement attained is used as the internal history parameter $\kappa$. The crack normal and tangential stiffnesses are then both made functions of the internal parameter. A loading function is defined as

$$f(\alpha_n, \kappa) = \alpha_n - \kappa \tag{22}$$

where $f \geq 0$ indicates loading (crack opening) and $f < 0$ indicates unloading (crack closing). A closed crack is indicated by $\alpha_n \leq 0$.

For modelling materials like concrete, an exponential softening curve is adopted for the normal traction–separation relationship. Using the fracture energy ($G_f$), tensile strength and internal history parameter gives the traction transfered across a discontinuity via

$$t_n = f_t \exp\left(-\frac{f_t}{G_f}\kappa\right). \tag{23}$$

The shear stiffness is given as an exponential function of the internal variable $\kappa$,

$$t_{s,t} = \mathrm{d_{int}} \exp(\mathrm{h_s}\kappa)\, \alpha_{s,t}\,, \tag{24}$$

where $\mathrm{d_{int}}$ is the initial shear stiffness of the crack ($\kappa = 0$) and $\mathrm{h_s}$ reflects the crack shear stiffness at some intermediate stage of damage.

Differentiating (23) and (24) with respect to time, a consistently linearised material tangent can be formed.

$$\begin{Bmatrix} \dot{t}_n \\ \dot{t}_s \\ \dot{t}_t \end{Bmatrix} = \begin{bmatrix} -\frac{f_t^2}{G_f}\exp(-\frac{f_t}{G_f}\kappa) & 0 & 0 \\ \mathrm{h_s d_{int}} \exp(\mathrm{h_s}\kappa)\alpha_s & \mathrm{d_{int}}\exp(\mathrm{h_s}\kappa) & 0 \\ \mathrm{h_s d_{int}} \exp(\mathrm{h_s}\kappa)\alpha_t & 0 & \mathrm{d_{int}}\exp(\mathrm{h_s}\kappa) \end{bmatrix} \begin{Bmatrix} \dot{\alpha}_n \\ \dot{\alpha}_s \\ \dot{\alpha}_t \end{Bmatrix}. \tag{25}$$

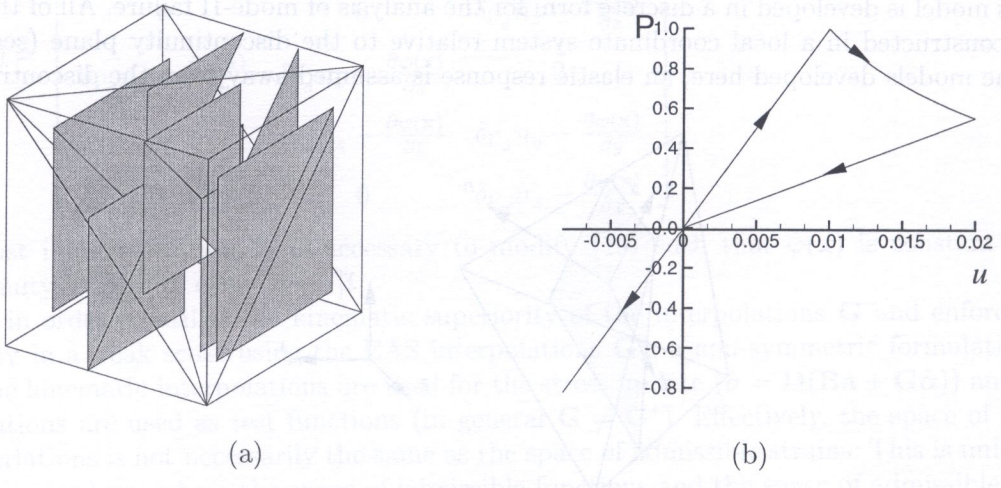


(a) (b)

**Fig. 4.** Unit patch of 12 four-noded tetrahedral elements (a) embedded discontinuity plane, (b) loading–unloading response

For unloading, the secant is used by simply making all off-diagonal terms equal to zero and replacing the (1,1) component of the tangent with $f_t \exp(-\frac{f_t}{G_f}\kappa)/\kappa$. To achieve elastic unloading, all diagonal terms can be made very large. Theoretically, since there is no elastic component at the discontinuity, the diagonal terms are infinitely large for elastic unloading.

Upon crack closure, full stiffness recovery for both normal and tangential components is assumed. This is done by making the stiffness very large in all directions. The loading and unloading behaviour for a cube of elements first pulled in tension and then compressed is illustrated in Fig. 4.

### 4.2. Associative plasticity

Contrary to the previous section where the discrete constitutive model was formed by directly considering the traction–separation relationships at the interface, here the formulation begins from a rate-independent elastoplastic continuum. The classical elastoplastic model is governed by the following relationships:

$$\dot{\boldsymbol{\sigma}} = \mathbf{C}{:}(\dot{\boldsymbol{\varepsilon}} - \dot{\boldsymbol{\varepsilon}}^p)\,, \tag{26a}$$

$$\dot{\boldsymbol{\varepsilon}}^p = \dot{\lambda}\,\partial_\sigma \phi\,, \tag{26b}$$

$$\dot{q} = -\dot{\lambda}\,H\,\partial_q \phi\,, \tag{26c}$$

$$\phi(\boldsymbol{\sigma}, q) = \hat{\phi}(\boldsymbol{\sigma}) + q - \bar{\sigma} \leq 0, \qquad \lambda \geq 0, \quad \lambda\,\phi(\boldsymbol{\sigma}, q) = 0\,, \tag{26d}$$

where $\boldsymbol{\sigma}$, $\boldsymbol{\varepsilon}$, $\boldsymbol{\varepsilon}^p$ are the stress, strain and plastic strain tensors, $\mathbf{C}$ is the elastic constitutive tensor, $\lambda$ is the plastic multiplier, $\phi(\boldsymbol{\sigma}, q)$ is a yield function, $\hat{\phi}(\boldsymbol{\sigma})$ is a homogeneous function of degree one, $q$ is a stress-like internal variable, $\bar{\sigma}$ is the yield stress and $H$ is the hardening modulus. The usual consistency equation ($\dot{\phi}(\boldsymbol{\sigma}, q) = 0$) is also imposed.

By considering that tractions must be continuous across any material discontinuity, it is possible to show that classical continuum relationships are compatible with strong discontinuities for strain softening problems. Effectively, if the softening modulus ($H$) has a distributional form, it cancels the unbounded Dirac-delta terms in the strain field (see Simo *et al.*, [12] for details). Also from the traction continuity condition it is also possible to develop conditions for the introduction of a discontinuity, although some questions exist over the exact condition for the inducement of a strong discontinuity [18].

#### *4.2.1. Displacement jump*

If the hardening modulus has a distributional form, this implies that the plastic multiplier must be unbounded. Defining a bounded form of the plastic multiplier ($\bar{\lambda}$) such that

$$\lambda = \delta\bar{\lambda}\,, \tag{27}$$

it is possible to substitute the unbounded part of the strain field from (5) into (26b) (at the discontinuity):

$$(\llbracket \dot{\mathbf{u}} \rrbracket \otimes \mathbf{n})^s = \bar{\lambda}\partial_\sigma \phi_{\Gamma_d}\,. \tag{28}$$

Considering the components of the basis of ($\llbracket \mathbf{u} \rrbracket \otimes \mathbf{n}$) in (7), it follows from (26a) that the components of stress at the discontinuity can be written:

$$\boldsymbol{\sigma}_{\Gamma_d} = \begin{bmatrix} \sigma_{nn} & \sigma_{ns} & \sigma_{nt} \\ \sigma_{ns} & 0 & 0 \\ \sigma_{nt} & 0 & 0 \end{bmatrix}. \tag{29}$$

This shows that the active stresses at the discontinuity surface can be resolved into three components. Note that any constitutive model that does not allow plastic volume change ($\mathrm{tr}(\dot{\boldsymbol{\varepsilon}}^p) = 0$)

reduces to a slip plane since the (1,1) component of (7) must be equal to zero. In this case the stress component normal to the discontinuity is purely elastic.

From the consistency condition it can be computed,

$$\dot{\bar{\lambda}} = \frac{\dot{\bar{\phi}}}{\bar{H}} \,. \tag{30}$$

Substituting the above result into (26b), the displacements at the discontinuity can be solved.

$$(\llbracket \dot{\mathbf{u}} \rrbracket \otimes \mathbf{n})^s = \frac{\dot{\bar{\phi}}}{\bar{H}} \, \partial_\sigma \phi \,. \tag{31}$$

### *4.2.2. Von Mises plasticity*

Attention is now focused on refining the strong discontinuity model for the special case of von Mises plasticity. The yield function is given by

$$\phi(\boldsymbol{\sigma}, q) = \sqrt{\frac{3}{2}} \, \|\mathbf{S}\| + q - \bar{\sigma} \tag{32}$$

where $\|\mathbf{S}\|$ is the norm of the deviatoric stress tensor. Differentiating the yield function with respect to stresses, it can be shown

$$\partial_\sigma \phi = \sqrt{\frac{3}{2}} \frac{\mathbf{S}}{\|\mathbf{S}\|} \,. \tag{33}$$

Since the volumetric plastic strain rate must be zero for von Mises plasticity, the discontinuity reduces to a slip plane with two independent stress components in the plane of the discontinuity. The deviatoric stress tensor can then be written:

$$\mathbf{S}_{\Gamma_d} = \begin{bmatrix} 0 & S_{ns} & S_{nt} \\ S_{ns} & 0 & 0 \\ S_{nt} & 0 & 0 \end{bmatrix} . \tag{34}$$

In order to calculate the displacement jumps using (31), the yield function can be differentiated with respect to time,

$$\dot{\bar{\phi}}_{\Gamma_d} = \sqrt{\frac{3}{\sigma_{ns}^2 + \sigma_{nt}^2}} \, (\sigma_{ns} \dot{\sigma}_{nt} + \sigma_{nt} \dot{\sigma}_{nt}) \,. \tag{35}$$

Considering (8) and substituting Eqs. (35) and (33) into (31), it can be shown

$$\begin{bmatrix} \llbracket \dot{u} \rrbracket_s \\ \llbracket \dot{u} \rrbracket_t \end{bmatrix} = \frac{3}{\bar{H}} \frac{1}{\sigma_{ns}^2 + \sigma_{nt}^2} \begin{bmatrix} \sigma_{ns}^2 & \sigma_{nt}\sigma_{nt} \\ \sigma_{ns}\sigma_{nq} & \sigma_{nt}^2 \end{bmatrix} \begin{bmatrix} \dot{\sigma}_{ns} \\ \dot{\sigma}_{nt} \end{bmatrix} . \tag{36}$$

Note that the determinant of the matrix on the RHS of (36) is equal to zero. This is because the displacement jump at the discontinuity can be expressed as $\llbracket \dot{\mathbf{u}} \rrbracket = \zeta \mathbf{m}$ where $\zeta$ is the magnitude of the jump and $\mathbf{m}$ is the direction of the jump displacement. Equation (36) can be manipulated to give $\zeta$:

$$\zeta = \| \, \llbracket \dot{\mathbf{u}} \rrbracket \, \| = \frac{3}{\bar{H} \sqrt{\sigma_{np}^2 + \sigma_{nq}^2}} \, (\sigma_{np} \dot{\sigma}_{np} + \sigma_{nq} \dot{\sigma}_{nq}) \,. \tag{37}$$

For numerical implementation, it is necessary to rearrange (36) to give the stress components in terms of displacements. For two-dimensional problems where a discontinuity reduces simply to a slip line, this can be done simply from (37) by considering only one component. For three-dimensional

problems, where a discontinuity results in a slip plane, it is necessary to integrate along the loading path [18]. This results in:

$$\sigma_i = \left( \sqrt{(\sigma_s^2 + \sigma_t^2)_{t=0}} + \frac{\bar{H}(\kappa)}{3} \kappa \right) \frac{[\![u]\!]_i}{\kappa}, \qquad i = s, t, \quad \kappa > 0, \tag{38}$$

for linear softening.

To model elastic unloading of the plasticity model, all components of the material tangent are made very large.

## 5. Numerical examples

To illustrate the numerical performance of embedded models in three-dimensions, examples of mode-I and mode-II failure are given. All the examples are performed using three-dimensional 4-noded tetrahedral elements and use the constitutive models developed in Section 4.

### 5.1. Shear layer

To analyse a shear layer (Fig. 5), the discrete von Mises model has been applied. The following material properties are adopted: $E = 1.0 \times 10^2$ MPa, $\bar{\sigma} = 1.0$ MPa, $\nu = 0.0$, $G_f = 0.1$ Nmm/mm$^2$. All boundary nodes are restrained in the longitudinal direction to avoid bending of the layer. One mesh is constructed with 45 elements while a second is constructed with 110 elements. To induce localised failure, elements in the centre of each bar have been weakened.

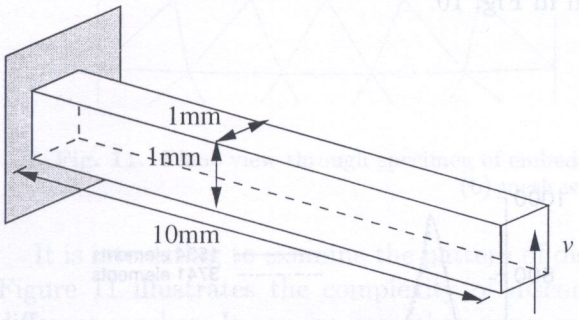


**Fig. 5.** Shear layer

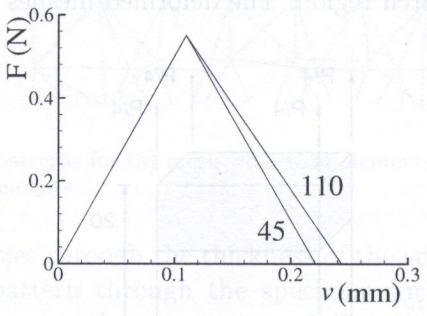


**Fig. 6.** Load–displacement response for shear layer with 45 elements and 110 elements

The load–displacement response of the two specimens in Fig. 6 shows that the response of the two meshes is almost identical. The small difference comes from the slightly different mesh structure of the two meshes. In the coarse mesh, only 11 elements were required to localise due to the packing of elements in the centre of the layer. The mesh with 110 elements has a slightly different packing of elements in the centre of the bar, requiring that 12 elements localise. This is due to the kinematic interaction (displacement compatibility) between elements. Figure 7 shows the deformed meshes and the embedded discontinuity planes for the two meshes. The mesh sensitivity shown in Fig. 6 is not consistent with the mesh sensitivity observed with classical continuum softening models where a finer mesh results in a more brittle response, with the limit case upon refinement failure with zero energy dissipation.

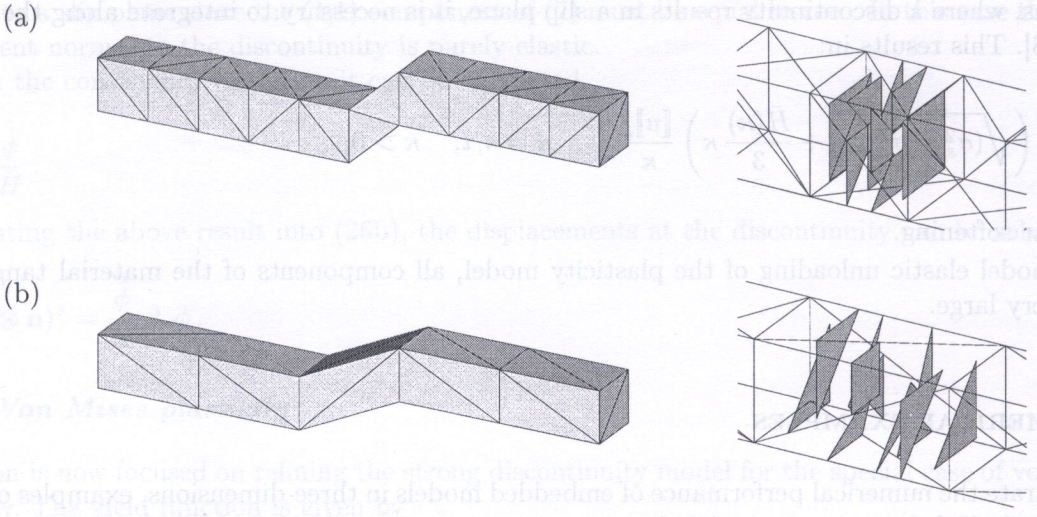


**Fig. 7.** Deformed mesh and embedded planes for (a) 110 elements and (b) 45 elements

### 5.2. Brittle fracture

To examine a more complex problem, a double notched specimen is tested in tension (Fig. 8) using the cohesive crack type model. The following material properties are adopted: $E = 1.0 \times 10^4$ MPa, $f_t = 1.0$ MPa, $\nu = 0.1$, $G_f = 0.02$ Nmm/mm$^2$, $d_{int} = 1.0 \times 10^2$ N/mm, $d_{\kappa=1.0} = 1.0 \times 10^{-6}$ N/mm. To avoid fracture at the top and bottom of the specimen, the load is applied through loading plates at the top and bottom of the specimen. Two different meshes are used to test the mesh objectivity of the method.

It can be seen from the global load–displacement response in Fig. 9 that two meshes produce nearly identical results. It should also be noted that the mesh with 1534 elements is unstructured in the notch region. The deformed meshes are shown in Fig. 10.

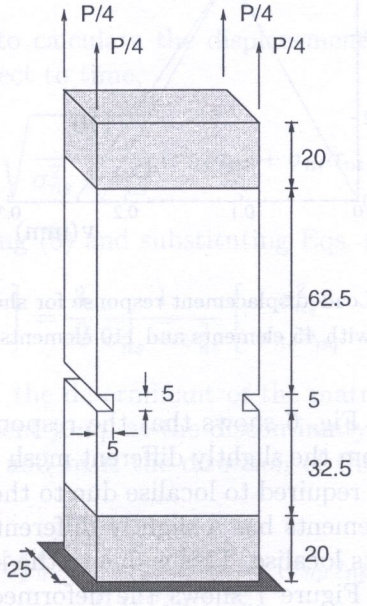


**Fig. 8.** Double notched specimen (loading plates shaded)

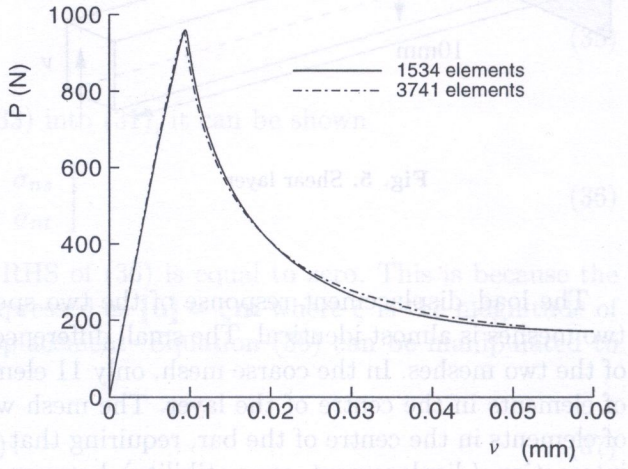


**Fig. 9.** Load–displacement response of double notched specimen

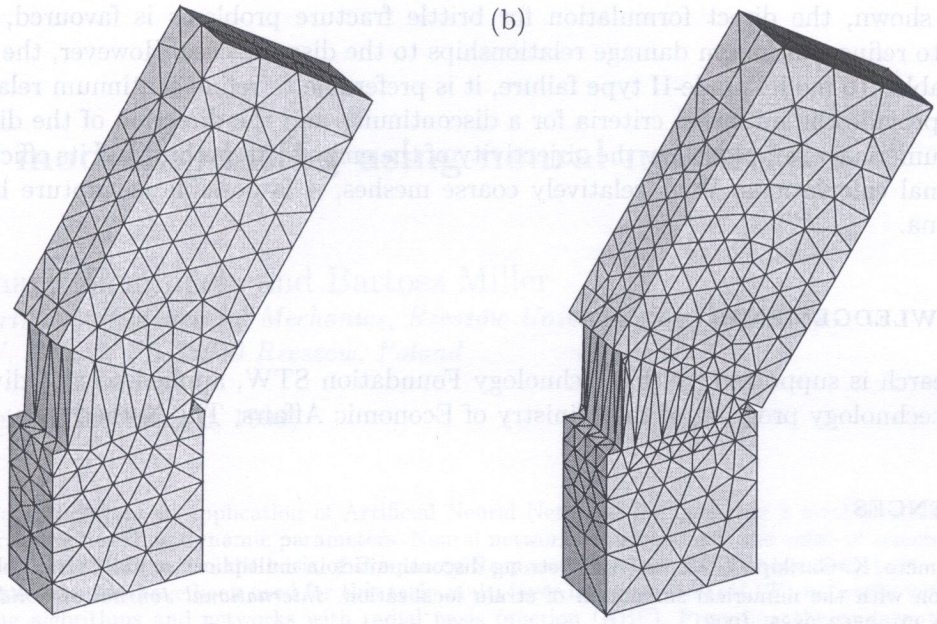


**Fig. 10.** Deformed specimen: (a) mesh with 1534 elements and (b) mesh with 3741 elements

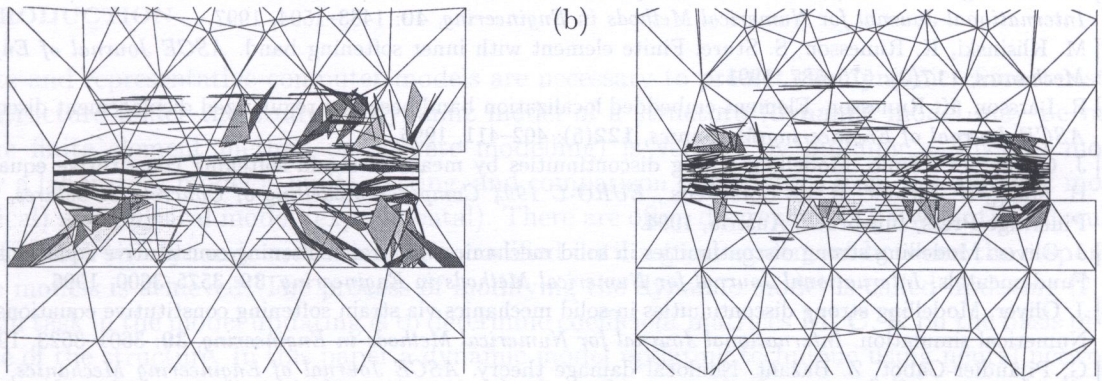


**Fig. 11.** Plane view through specimen of embedded crack patterns for (a) mesh with 1534 elements and (b) mesh with 3741 elements

It is interesting to examine the pattern of discontinuities through the thickness of the specimens. Figure 11 illustrates the complexity of discontinuity pattern through the specimen for the two different meshes. It can be seen that upon mesh refinement, the orientation of discontinuities is better captured since the stress field is more accurate, especially near the notches of the specimen.

## 6. Conclusions

The application of embedded strong discontinuity models has been shown, from the development of a finite element that includes discontinuous, incompatible strain modes to discrete constitutive models for mode-I and mode-II failure. The method overcomes many of the problems of classical continuum models. By maintaining Dirac-delta distributions through the derivation and their explicit integration, no numerical parameters are required in the constitutive model to avoid element size dependency, nor are they required to approximate the Dirac-delta distribution with a bounded function.

It has been shown that discrete constitutive models can be either formulated directly in terms of tractions and displacements or they can be refined from continuum relationships. For the mode-I

example shown, the direct formulation for brittle fracture problems is favoured, although it is possible to refine continuum damage relationships to the discrete case. However, the value of this is questionable. To model mode-II type failure, it is preferable to refine continuum relationships since this can provide the initiation criteria for a discontinuity and the direction of the discontinuity.

The numerical examples show the objectivity of the embedded method and its efficiency for three-dimensional calculations. With relatively coarse meshes, it is possible to capture highly localised phenomena.

## Acknowledgements

This research is supported by the Technology Foundation STW, applied science division of NWO and the technology program of the Ministry of Economic Affairs, The Netherlands.

## References

[1] F. Armero, K. Garikipati. An analysis of strong discontinuities in multiplicative finite strain plasticity and their relation with the numerical simulation of strain localization. *International Journal of Solids and Structures*, **33**(20-22): 2863–2885, 1996.

[2] R. de Borst, H.B. Mühlhaus. Gradient-dependent plasticity – formulation and algorithmic aspects. *International Journal for Numerical Methods in Engineering*, **35**(3): 521–539, 1992.

[3] M. Fleming, Y.A. Chu, B. Moran, T. Belytschko. Enriched element-free Galerkin methods for crack tip fields. *International Journal for Numerical Methods in Engineering*, **40**: 1483–1504, 1997.

[4] M. Klisinski, K. Runesson, S. Sture. Finite element with inner softening band. *ASCE Journal of Engineering Mechanics*, **117**(3): 575–587, 1991.

[5] R. Larsson, K. Runesson. Element-embedded localization band based on regularized displacement discontinuity. *ASCE Journal of Engineering Mechanics*, **122**(5): 402–411, 1996.

[6] J. Oliver, J.C. Simo. Modelling strong discontinuities by means of strain softening constitutive equations. In H. Mang, N. Bićanić, R. de Borst, eds., *EURO-C 1994 Computer Modelling of Concrete Structures*, 363–372. Pineridge Press, Innsbruck, Austria, 1994.

[7] J. Oliver. Modelling strong discontinuities in solid mechanics via strain softening constitutive equations. Part 1: Fundamentals. *International Journal for Numerical Methods in Engineering*, **39**: 3575–3600, 1996.

[8] J. Oliver. Modelling strong discontinuities in solid mechanics via strain softening constitutive equations. Part 2: Numerical simulation. *International Journal for Numerical Methods in Engineering*, **39**: 3601–3623, 1996.

[9] G. Pijaudier-Cabot, Z. Bažant. Nonlocal damage theory. *ASCE Journal of Engineering Mechanics*, **113**(10): 1512–1533, 1987.

[10] J.G. Rots. *Computational Modeling of Concrete Fracture*, Ph.D. thesis, Delft University of Technology, 1988.

[11] J.C. Simo, M.S. Rifai. A class of mixed assumed strain methods and the method of incompatible modes. *International Journal for Numerical Methods in Engineering*, **29**: 1595–1638, 1990.

[12] J.C. Simo, J. Oliver, F. Armero. An analysis of strong discontinuities induced by strain-softening in rate-independent inelastic solids. *Computational Mechanics*, **12**: 277–296, 1993.

[13] L.J. Sluys, *Wave Propagation, Localisation and Dispersion in Softening Solids*, Ph.D. thesis, Delft University of Technology, 1992.

[14] D.V. Swenson, A.R. Ingraffea. Modeling mixed-mode dynamic crack propagation using finite elements: Theory and applications. *Computational Mechanics*, **3**: 381–397, 1988.

[15] R.L. Taylor, J.C. Simo, O.C. Zienkiewicz, C.H. Chan. The patch test – a condition for assessing FEM convergence. *International Journal for Numerical Methods in Engineering*, **22**: 39–62, 1986.

[16] G.N. Wells, L.J. Sluys. Application of embedded discontinuities for softening solids. *Engineering Fracture Mechanics*, **65**(2-3): 263–281, 2000.

[17] G.N. Wells, L.J. Sluys. Three-dimensional embedded discontinuity model for brittle fracture. *International Journal of Solids and Structures* (in print).

[18] G.N. Wells, L.J. Sluys. Analysis of slip planes in three-dimensional solids. *Computer Methods in Applied Mechanics and Engineering* (in print).